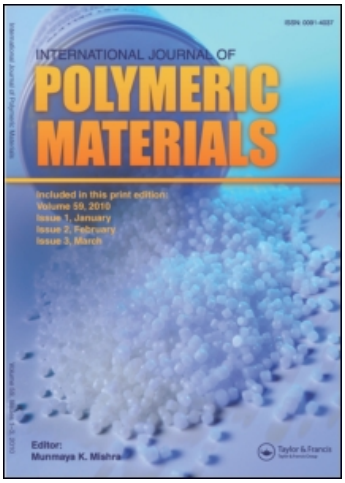

International Journal of Polymeric Materials
Publication details, including instructions for authors and subscription information:
http://www.informaworld.com/smpp/title~content=t713647664

Dynamics of the Parachute Sling: Testing Procedures and Evaluations

D. C. Prevorsek[a]; H. B. Chin[a]; Y. D. Kwon[a]
[a] Allied-Signal Inc., Research and Technology, Morristown, NJ

To cite this Article Prevorsek, D. C. , Chin, H. B. and Kwon, Y. D.(1994) 'Dynamics of the Parachute Sling: Testing Procedures and Evaluations', International Journal of Polymeric Materials, 25: 3, 143 — 159
To link to this Article: DOI: 10.1080/00914039408029335
URL: http://dx.doi.org/10.1080/00914039408029335

Intern. J. Polymeric Mater., 1994, Vol. 25, pp. 143–159
Reprints available directly from the publisher
Photocopying permitted by license only

Printed in Malaysia

Dynamics of the Parachute Sling: Testing Procedures and Evaluations

D. C. PREVORSEK, H. B. CHIN and Y. D. KWON

Allied-Signal Inc., Research and Technology, P.O. Box 1021, Morristown, NJ 07962-1021

(Received September 20, 1993)

This paper discusses material science aspects of a parachute sling. During the deployment of a parachute, the sling experiences the impact caused by rapid deceleration of the parachute. To survive this operation, the sling must have sufficient impact resistance in addition to the strength to withstand the tension due to the weight of payload. The amount of energy absorbed by the sling due to the impact was estimated from the dynamic analysis of a parachute. From the results of the dynamic analysis, the key properties required for a sling material were determined and testing procedures to evaluate those properties were established. The experimental evaluation results for two candidate materials are presented.

KEY WORDS Parachute, sling, webbing, dynamics, nylon

INTRODUCTION

The dynamic behavior of parachute systems has been investigated by many researchers theoretically and experimentally to varying degrees of complexity. The major problems include the prediction of aerodynamic forces acting on the parachute canopy, complexity of analyzing the flow field around the parachute, and dynamic instability of parachute system. Especially, the inflation stage poses a serious problem because the aerodynamic forces acting on the parachute depend on the shape of its canopy but the shape of the canopy depends on the air flow which affects the aerodynamic forces. In addition, as the canopy opens, the parachute decelerates rapidly dissipating its kinetic energy into kinetic energy of air molecules. This in turn increases the strain energy of the parachute components such as the sling. Each of these phenomena involved in parachute deployment is difficult to analyze theoretically and requires a good understanding of underlying principles.

In order to predict the exact behavior of a parachute, one has to solve simultaneously the equations of motion for the parachute and the equations of motion for the air around the parachute. However, it is not the purpose of this study to analyze the exact behavior of the parachute but to analyze the effect of parachute behavior on the static and dynamic behavior of the sling. Thus we simplified the analysis, focussing on the function of parachute sling and neglecting certain pa-

rameters which are not important in the behavior of the sling during parachute deployment.

Using such an approach we developed a mathematical model to predict the parachute behavior and to estimate the magnitude of strain energy and stresses in the sling. The output of the model was verified using experimental data. Then the key material property criteria for the sling were determined and proper testing procedures were established.

The primary objectives of this study were:

a. To estimate the magnitude and history of strain energy that the sling will experience during the inflation and steady descent phases of the deployment
b. To determine key factors affecting the magnitude of strain energy of the sling
c. To identify key material properties for the selection of sling material
d. To establish proper testing methods to select the best candidate material

In this paper, the results of our analysis, the material property criteria, and testing procedures and testing results of potential sling materials are presented.

DYNAMIC ANALYSIS

As pointed out above, the behavior of a parachute system during the inflation stage is extremely complex, thus the bulk of theoretical studies reported in the literature has been on the analysis of dynamic behavior and stability of fully deployed (opened) parachutes.[1-5] Therefore, to investigate the role and material aspects of the sling, we solved the equations of motion for the inflation and steady descent stages of a parachute system, using estimated aerodynamic forces by approximation rather than solving complicated air flow around the parachute. The results of our analysis were then compared with data obtained from actual deployment experiments to improve the accuracy of the solution. From the analysis, we investigated the effects of various deployment variables on the sling during inflation and steady descent stages.

EQUATIONS OF MOTION

The equations of motion for the parachute system are based on Newton's laws of motion. To simplify the problem, the parachute system is idealized while retaining the realistic aspects. It is assumed that:

a. The parachute system consists of an axisymmetric parachute (canopy and suspension lines), sling and payload (cargo). The sling is rigidly connected to the parachute.
b. The air density is constant.
c. The aerodynamic forces acting on the parachute and payload are functions of translational velocity of the parachute.

Based on the above assumptions, the general equations of motion for the parachute system can be written using the Lagrangian equations of motion as,

$$\frac{d}{dt}\left(\frac{\partial T}{\partial v_i}\right) + \varepsilon_{ijk}\Omega_j\left(\frac{\partial T}{\partial v_k}\right) = F_i \tag{1}$$

$$\frac{d}{dt}\left(\frac{\partial T}{\partial \Omega_i}\right) + \varepsilon_{ijk}\Omega_j\left(\frac{\partial T}{\partial \Omega_k}\right) + \varepsilon_{ijk}v_j\left(\frac{\partial T}{\partial v_k}\right) = M_i \tag{2}$$

where T is the kinetic energy of the system and t is time. v_i and Ω_i are linear and angular velocities, and F_i and M_i are the external forces and moments acting on the parachute system, respectively.

Since we are mainly concerned with the stresses and strain energy in the sling, we will further simplify the analysis of the parachute behavior. For the case when the motion of parachute is symmetric about the x-z plane in reference to Figure 1, the component equations of the equations of motion (Equations 1 and 2) can be written as[6]:

$$(m + \alpha_{11})\dot{U} + (mZ_s + \alpha_{15})\dot{Q} + (m + \alpha_{33})QW = F_x \tag{3}$$

$$(m + \alpha_{33})\dot{W} - (m + \alpha_{11})QU - (mZ_s + \alpha_{15})Q^2 = F_z \tag{4}$$

$$(I_{yy} + \alpha_{55})\dot{Q} + (mZ_s + \alpha_{15})(\dot{U} + QW) - (\alpha_{11} - \alpha_{33})UW = M_y \tag{5}$$

where m is the mass of the system and α_{ij} are the components of apparent mass tensor. U and W are linear velocity components along the x and z axes and Q is the angular velocity component about the y axis. I_{yy} is the moment of inertia of the system and F_x, F_z and M_y are the external force components along the x and z axes and moment about the y axis, respectively. Z_s is the distance along the z axis from the origin of the coordinates to the mass center. The upper dot denotes differentiation with respect to time.

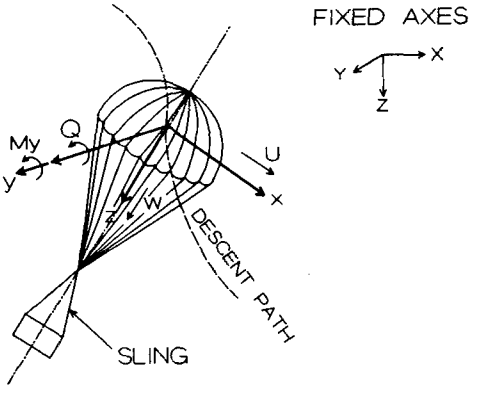

FIGURE 1 Fixed and moving systems of axes.

The apparent mass, sometimes referred to as virtual mass, is a tensor quantity varying in magnitude as the direction of the body motion changes. The component of the apparent mass is generally related to the mass of the fluid displaced by the body. Thus the components of the apparent mass tensor are expressed using the concept of the apparent (or virtual) mass coefficient, K_{ij}, hence,

$$\alpha_{11} = K_{11}\rho V \tag{6}$$

$$\alpha_{33} = K_{33}\rho V \tag{7}$$

$$\alpha_{55} = K_{55}I_f \tag{8}$$

$$V = \pi D_0^3/12 \tag{9}$$

$$I_f = D_0^2\rho V/16 \tag{10}$$

where D_0 is the nominal diameter of the parachute canopy and ρ is the density of air.

Note that for axisymmetric parachute systems, only four components of the apparent mass tensor are independent, i.e., α_{11}, α_{33}, α_{55} and α_{15}. The values of these components vary depending on the type of parachutes and they can be determined experimentally using a wind tunnel. Yavuz[7] showed that, if the coordinate system origin is at the canopy center of pressure, then $\alpha_{15} = 0$.

The main external forces consist of gravity, aerodynamic forces acting on the parachute and drag force acting on the payload, i.e.,

$$F_x = -mg \sin\theta - (F_{bx} + F_{px}) \tag{11}$$

$$F_z = mg \cos\theta - (F_{bz} + F_{pz}) \tag{12}$$

$$M_y = -mg \sin\theta\, Z_s - F_{px}Z_r \tag{13}$$

in which F_{px} and F_{pz} are the aerodynamic force components along the x and z axes and F_{bx} and F_{bz} are the drag force components acting on the payload along the x and z axes, respectively. The drag force can be approximately determined using particle dynamics as:

$$F_{bx} = \frac{C_D A_p \rho V_t^2}{2g_c} \sin\beta, \qquad F_{bz} = \frac{C_D A_p \rho V_t^2}{2g_c} \cos\beta \tag{14}$$

Similarly, the aerodynamic force is estimated based on the assumption that the force acting on the parachute is proportional to the square of the parachute velocity and the projected canopy area, i.e.,

$$F_{px} = \frac{C_A \pi D^2 V_t^2}{4} \cos\beta \sin\beta, \qquad F_{pz} = \frac{C_A \pi D^2 V_t^2}{4} \cos^2\beta \tag{15}$$

in which C_A can be determined from the steady descending velocity for the parachute. It is further assumed that, during the parachute opening stage, the increase of parachute diameter can be expressed as a function of time, by

$$D = D_0 \left(\frac{t}{t_0}\right)^2, \qquad \text{for} \qquad t \leq t_0 \tag{16}$$

The velocity and rotation of the parachute are then determined from the relation of the stationary (fixed) coordinates and the moving coordinates with the parachute:

$$\dot{\theta} = Q \tag{17}$$

$$\dot{X} = U \cos \theta + W \sin \theta \tag{18}$$

$$\dot{Z} = -U \sin \theta + W \cos \theta \tag{19}$$

Equations 1 through 19 constitute the relationships governing the dynamic behavior of the parachute system.

TENSION AND ENERGY ABSORBED IN THE SLING

The tension in the sling is generated by the aerodynamic force acting on the parachute and thus is balanced with the aerodynamic force. Hence, the tension, σ_t can be given by

$$\sigma_t = F_{pz} \tag{20}$$

The energy absorbed by the sling can then be calculated from the tension and the stress-strain relationship of the sling material.

RESULTS OF ANALYSIS

These governing equations were solved numerically using the fourth order Runge-Kutta method subject to appropriate initial conditions. The solution of these equations enables us to determine the magnitude of strain energy and stresses in the sling and material properties required for the sling. Also the analysis results can be used to select and optimize the material and to develop testing procedures in consideration of various parachute deployment parameters.

Some results are presented in Figures 2 through 4. The key parameters affecting the dynamic behavior of a parachute include the aircraft speed, duration of parachute opening and delay of parachute opening. The aircraft speed has a significant effect on the tension of the sling and the amount of energy absorbed by the sling is largely influenced by the parachute opening process.

Figure 2 depicts the simulated trajectory of an 8 parachute cluster with 42,000

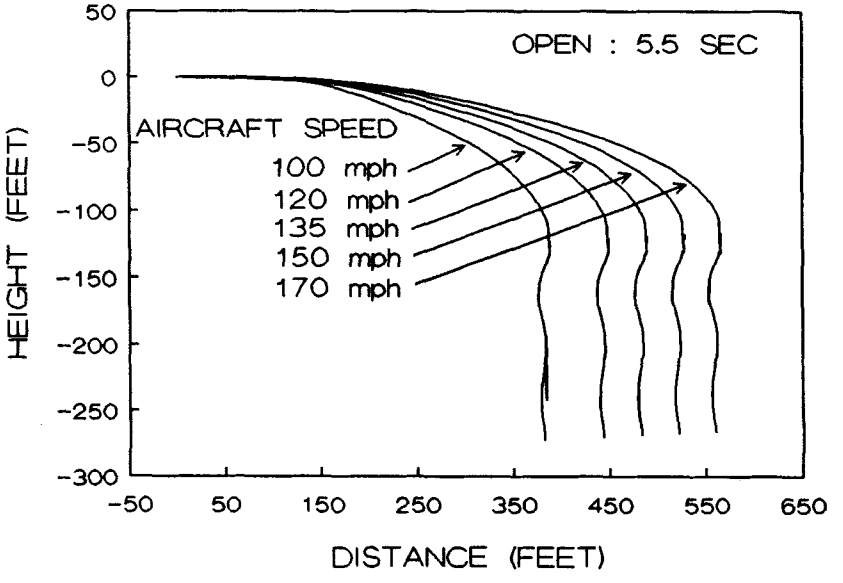

FIGURE 2 Predicted trajectory of parachute.

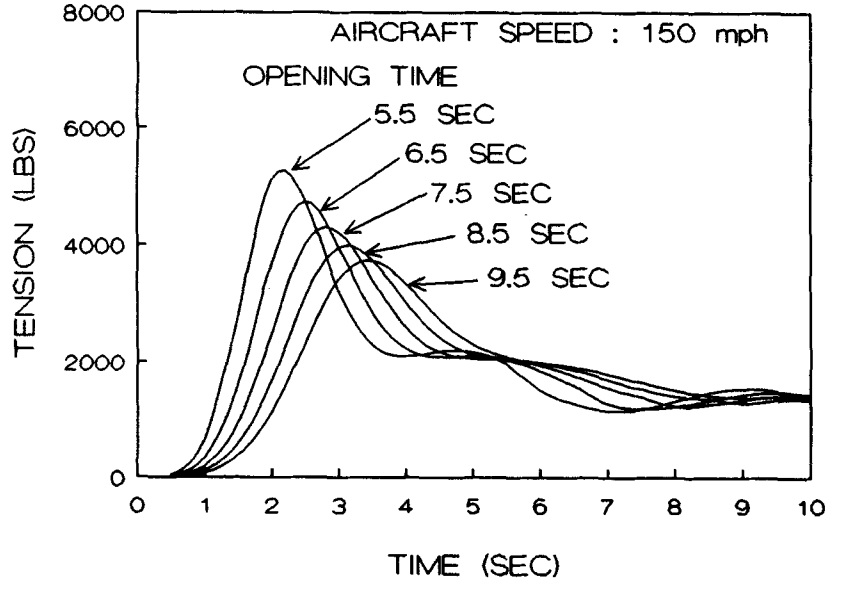

FIGURE 3 Predicted tension in sling.

pound payload. In Figure 3, the tension in the sling is shown. As can be seen, the tension during the early parachute opening phase is much higher than that during the steady descending period. As a result, the sling experiences a strong impact and absorbs the impact energy as shown in Figure 4.

The analysis results show that during the parachute opening, the aerodynamic force acting on the canopy increases rapidly, resulting in sudden deceleration, which

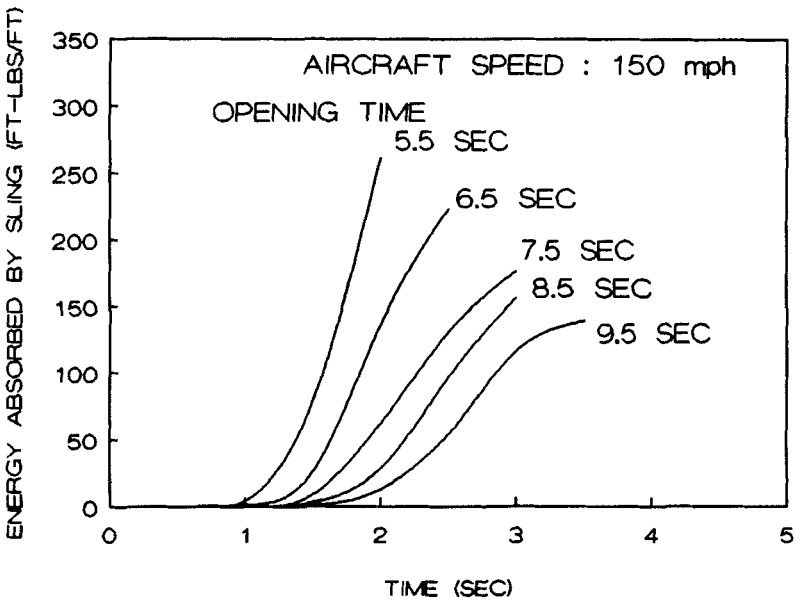

FIGURE 4 Predicted energy absorbed by sling (per ply webbing).

causes impact on the sling. The faster the parachute opens, the greater the impact energy. Consequently, the material used for the sling must have, in addition to sufficient strength, also high energy absorption capability. However, with current webbing constructions the strength criteria are much easier to meet than the energy absorption criteria. Therefore, the energy absorption capability must be recognized as one of the critical property requirements for the sling material.

VALIDATION OF MODEL

The analysis results were compared with experimental data to verify the validity of our mathematical model. In Figure 5, the predicted tension in the sling is compared with the experimentally measured tension during actual deployment at an aircraft speed of approximately 150 miles per hour. As can be seen, the magnitude of predicted tension is in good agreement with the measurement. Note that the cyclic variation of tension in the measurement is due to the swaying of the payload, which was not considered important in our analysis.

MATERIAL PROPERTY CRITERIA

Based on our analysis, we determined the following key material property criteria for the selection of sling material:

- Temperature rise under friction, impact or cyclic load
- Strength

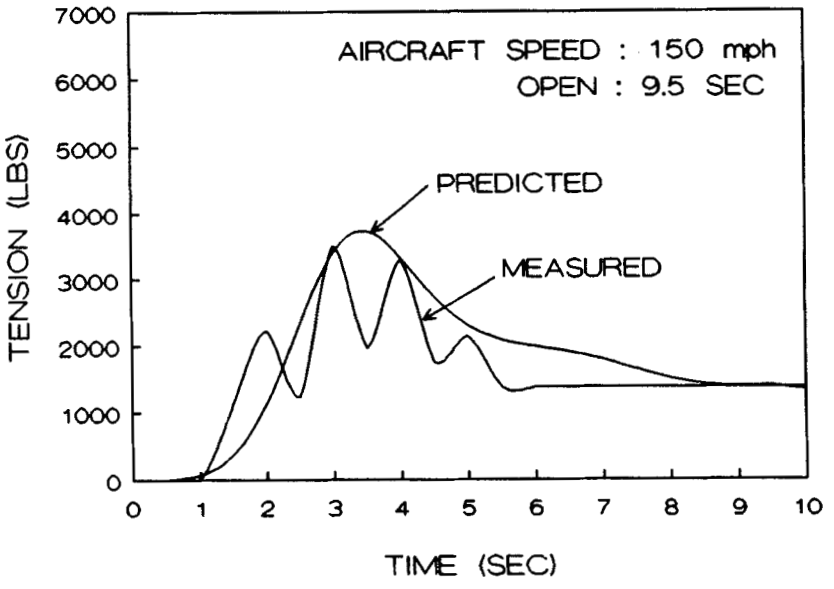

FIGURE 5 Comparison of predicted and measured tension in sling.

- Energy-to-break (energy absorption capacity)
- Strength and Energy-to-break loss on repeated use

The sling material should withstand the temperature rise due to surface friction so that its strength will not be impaired. The next concern is the temperature rise due to viscoelastic loss and friction under cyclic or impact loads. Low viscous dissipation and friction characteristics are desirable for the sling material. In regard to mechanical properties, the material used for the sling must have high energy absorption capability as well as sufficient strength.

Since the sling is designed for repeated use, the final consideration is the damage tolerance and property retention on repeated loadings. In general, the damage caused by the application of loads is a function of the ratio of the loads to the material capacities, e.g., ratio of energy absorbed to energy-to-break. The higher the ratio gets, the greater the damage becomes. Materials with higher energy-to-break tend to have higher damage tolerance.

In order to evaluate the material with respect to these criteria, we developed the testing procedures as described below.

PROPOSED TESTING PROCEDURES

In the process of airdropping heavy equipment by parachute, the sling, which is made of multiple piles of webbing, is subjected to a loading history which can be divided into the following four major categories:

a. Frictional wear (The webbing stored in the storage container is pulled out with surface rubbing against itself and against the surface of metallic fixture and equipment parts).

b. Tensile impact with bending over sharp edge (The impact occurs when the equipment is pulled out of the aircraft and goes into the state of suspension from the parachute).
c. Oscillating tensile load (This occurs while the payload suspended from the parachute sways and undergoes stabilization process).
d. Heating caused by friction, impact and oscillating loads.

In view of this loading history, the main concern regarding the performance of the sling is how durable the webbing material is against repeated use in the parachute deployment process. Therefore, the following testings were chosen:

- Characterization of the performance of webbing in friction against steel with rough surface
- Characterization of the performance of webbing against tensile impact
- Characterization of the performance of webbing against oscillating load
- Heat generation characteristics by friction, impact and oscillating loads
- Assessment of overall performance
- Cumulative damage analysis

The testing procedures used are described below.

FRICTION AGAINST STEEL

When the webbing is pulled out of its stored state in the beginning of deployment process, the webbing is rubbed against itself and against metallic fixture. The stresses and strains in the webbing during this part of deployment process are not known. Repetition of this process, however, could lead to a substantial decrease in strength of webbing because of frictional wear.

To simulate these frictional wear conditions experimentally, we chose the Method 5309 of Federal Standard FED-STD-191A (Frictional abrasion test). The webbing was subjected to this test and the tensile properties were measured before and after the testing to determine the extent of decrease in tensile properties caused by the frictional wear. During the testing, webbing temperature was also monitored. The testing conditions are shown in Table I.

TENSILE IMPACT

With regard to the tensile impact on the webbing during the deployment process, the following conditions were adopted:

TABLE I
Frictional abrasion test conditions

Friction medium: Hexagonal bar
Friction cycle: 60 ± 2 strokes/min (30 ± 1 cycles/min)
Total stroke: 5,000 (2,500 cycles)
Load: 5.2 lbs ± 2 oz
Single stroke: 12 ± 1 inches
No. of specimens: 5

- Single ply webbing sample
- 90° wrap angle over 1/8 inch radius (steel edge)
- 5,000 lb_f dynamic tensile load, onset rate of 5,000 lb_f/sec
- Impacted area to be tensile tested to failure at normal strain rate

An MTS 810 hydraulic testing machine with a specially designed fixture was used. The webbing specimen was held in a self-tightening clamp at one end, threaded over the edge with a radius of 1/8 inch at an angle of 90°, and clamped at the other end as shown in Figure 6. The load was applied by moving the fixture at the speed which would give a loading rate of 5,000 lb_f/sec.

Each test specimen was exposed to 10 consecutive high speed impact loadings at the same location. During the testing, the temperature rise caused by impact loading was measured by inserting a thermocouple at the center of the webbing specimen at the impact point. After 10 cycles of impact loading, the residual strength of webbing was measured to determine the degree of damage.

OSCILLATING LOAD

Because of swaying of the payload during stabilization after the parachute is released, the webbing experiences an oscillating load. The test simulating the oscillating load during parachute deployment was conducted by imposing 7 cycles of cyclic loading between 150 lb_f and 3,500 lb_f per ply. Tensile properties of the webbing were measured before and after cyclic stressing. The hysteresis loop area was measured from the corresponding plots to estimate the effect of hysteresis on webbing yarn temperature.

HEAT GENERATION

In the surface friction against steel and the impact loading of 90° wrap angle over 1/8 inch radius, heat is generated at the surface by the frictional work. In the case

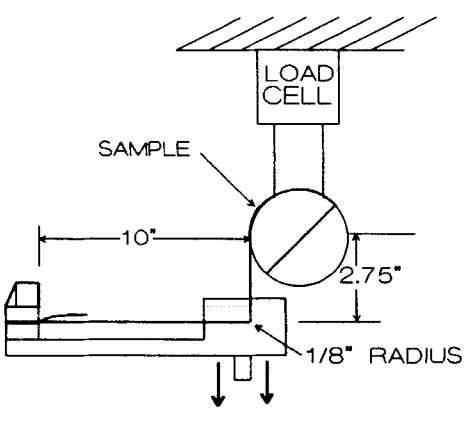

FIGURE 6 Schematic diagram of tensile impact tester.

of the oscillating load, viscoelastic hysteresis in the fiber causes self heating of the fiber and the interfilament friction generates heat, which also contributes to the temperature rise.

If the temperature rise in the webbing exceeds 50°C, it would significantly affect the mechanical properties of the webbing. Reduced modulus due to temperature increase could thus result in increased elongation or creep under load, accelerating the failure process. Therefore, it is important to monitor and understand the magnitude of temperature rise and its effect on webbing performance. The degree of temperature rise was measured subject to the frictional abrasion, tensile impact and oscillating loads.

EVALUATION OF TESTING PROCEDURES

Two candidate materials for sling were selected to test the testing procedures (Nylon 6 and Nylon 66). The respective webbings were then constructed to the military specification MIL-W-4088 type XXVI (dyed green and resin-treated) and tested as follows:

FRICTION AGAINST STEEL

Table II shows the tensile properties of Nylon 6 and Nylon 66 webbings before and after the frictional abrasion. As seen in Table II, during the frictional abrasion test, both webbings experienced strength loss but the strength reduction in Nylon 66 webbing appears greater. As to the energy-to-break, Nylon 66 webbing shows somewhat lower values than Nylon 6 webbing both before and after the abrasion.

TENSILE IMPACT

Table III shows the testing conditions and the residual tensile strength of Nylon 6 and Nylon 66 webbings. In this table, the impact load, maximum loading rate and

TABLE II

Effect of frictional abrasion (average values of 5 samples)

Items	Nylon 6	Nylon 66
Before the frictional abrasion		
Tensile strength, lb_f	15,500	17,900
Elongation to break, %	35.5	28.0
Energy-to-break, lb-in/in	2,310	1,710
After the frictional abrasion		
Tensile strength, lb_f	15,000	13,100
Elongation to break, %	34.1	23.8
Energy-to-break, %	2,150	1,010
Change in tensile strength, %	−3.2	−26.8
Change in energy-to-break, %	−6.9	−40.9

TABLE III

Effect of tensile impact (average values of 5 samples)

Items	Nylon 6	Nylon 66
Max. load during impact, lb_f		
Cycle 1	4,936	5,400
Cycle 10	4,779	5,512
Average loading rate, lb_f/sec		
Cycle 1	5,539	5,285
Cycle 10	5,838	5,944
Max. loading rate, lb_f/sec		
Cycle 1	7,299	7,191
Cycle 10	6,380	8,123
Residual tensile properties after 10 cycles of impact loading		
Tensile strength, lb_f	13,610	13,000
Change in tensile strength, %	−12.2	−27.4
Energy-to-break, lb-in/in	1,140	730
Change in energy-to-break, %	−50.6	−57.3

TABLE IV

Effect of oscillating load

Items	Nylon 6	Nylon 66
Webbing strength		
before cyclic stressing, lb_f	15,983	17,233
after 7 cyclic stressing, lb_f	14,583	15,993
Strength loss during the cylic stressing, %	−8.8	−7.2
Mechanical loss measured from the hysteresis loop (J/g)	1.6	1.18

TABLE V

Temperature rise

Items	Nylon 6	Nylon 66
Temperature rise due to friction, °C after 2500 abrasion cycles	13.2	14.8
Temperature rise due to impact, °C		
after cycle 1	5.0	10.6
after cycle 10	27.8	33.3
Max. temperature rise expected, °C after 7 cycles (cyclic load)	6.2	4.9

TABLE VI

Load bearing translation efficiency

Items	Nylon 6	Nylon 66
Yarn strength, g/den	8.03	9.37
Webbing denier, 10^6	1.26	1.26
Webbing strength projected from yarn strength, lb_f	22,270	26,000
Actual webbing stength, lb_f	15,500	17,900
Translation efficiency, %	69.6	68.9

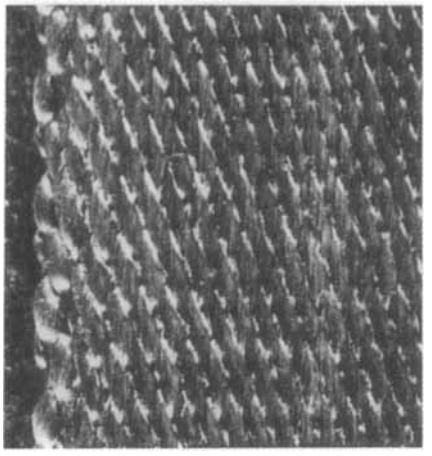

Nylon 6 webbing

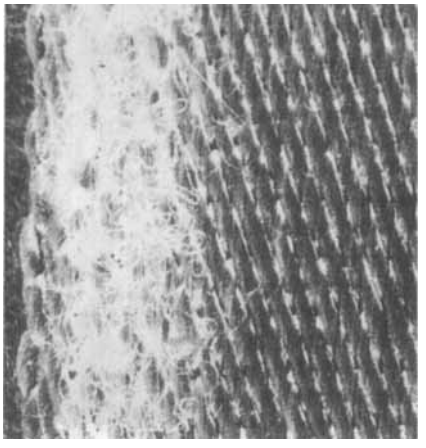

Nylon 66 webbing

FIGURE 7 Micrographs of webbings after friction test.

average loading rate of the first and last cycles are shown. An impact load of 5,000 lb_f was applied at an average loading rate of 5,000 lb_f/sec.

As can be seen in Table III, both webbings experienced strength reduction but much higher strength loss was observed with Nylon 66 webbing than Nylon 6 webbing. The higher strength loss in Nylon 66 is attributed to the lower bending fatigue resistance and higher friction coefficient of Nylon 66.

OSCILLATING LOAD

The testing under an oscillating load was conducted by applying a cyclic stress to the webbing. The gauge length of the sample was 4 inches and the straining rate

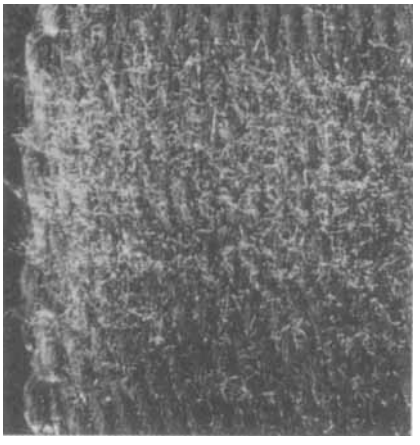

Nylon 6 webbing

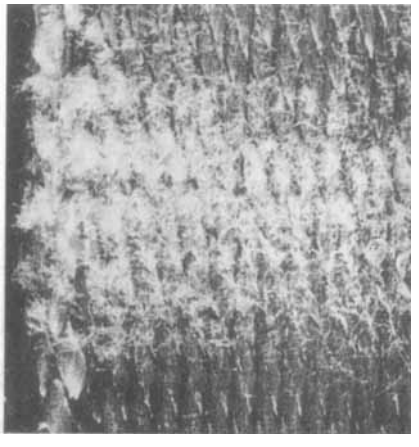

Nylon 66 webbing

FIGURE 8 Micrographs of webbings after tensile impact.

was 2 inches/min. During the cyclic stressing between 150 lb_f/webbing and 3,500 lb_f/webbing, the viscoelastic hysteresis loop was also drawn to determine the mechanical loss. Table IV shows the results of the measurements.

HEAT GENERATION

Table V shows the temperature rise in the webbing due to the friction, tensile impact and oscillating loads. The temperature rise, in general, is higher in the Nylon 66 webbing than the Nylon 6 webbing. This is attributed to the higher friction coefficient of Nylon 66. The higher temperature rise should affect adversely the retention of mechanical properties.

TABLE VII

Cumulative damage effect

Items	Nylon 6	Nylon 66
Strength retention in frictional abrasion (Table II)	0.968	0.732
Energy-to-break retention in frictional abrasion (Table II)	0.931	0.591
Strength retention in impact (Table III)	0.878	0.726
Energy-to-break retention in impact (Table III)	0.494	0.427
Strength retention in cyclic stressing (Table IV)	0.912	0.928
Cumulative strength retention (product of above 3 retentions)	0.775	0.493
Cumulative energy-to-break retention (product of above 2 retentions)	0.460	0.252

ASSESSMENT OF OVERALL PERFORMANCE

Table VI shows translation efficiency of yarn. As seen from this table, it appears that the translation efficiency seems to be almost the same for both Nylon 6 and 66 webbings.

SURFACE DAMAGE OF WEBBINGS

As discussed above, both Nylon 6 and Nylon 66 webbings suffered some damage due to friction (hex-bar abrasion) and tensile impact loads, however, the Nylon 66 was more susceptible to damage for both hex-bar abrasion and tensile impact.

Figures 7 shows micrographs of damaged areas of the Nylon 6 and Nylon 66 webbings exposed to the hex-bar abrasion. It is clearly seen that the Nylon 66 webbing underwent a large degree of surface damage whereas the Nylon 6 webbing experienced mild surface damage. A similar trend was observed with the webbings exposed to the tensile impact test (see Figure 8).

CUMULATIVE DAMAGE EFFECT

In the preceding sections, we examined the effect of each loading type on the change of webbing tensile properties. When these loadings occur in sequence, the damages accumulate in an additive fashion. Therefore, to comprehend the overall effect of the deployment process on the strength of webbing, the damage by each loading type has to be accounted for. Table VII summarizes the consideration of this cumulative damage effect for Nylon 6 and Nylon 66 webbings.

Table VII shows that the Nylon 6 webbing outperforms the Nylon 66 webbing in the strength retention and energy-to-break retention after the cumulative damage. The superior performance of Nylon 6 webbing in cumulative effect of friction abrasion, tensile impact and oscillating loads may have resulted largely from the differences in morphological structure between Nylon 6 and Nylon 66 fibers. Work is in progress to identify the key structural characteristics affecting the mechanical

behavior of these fibers. The results of this study will be reported in a separate article.

CONCLUDING REMARKS

Based on the results of our study, the following conclusions can be drawn.

1. An analytical procedure was developed yielding the tension and strain energy history of the sling during parachute deployment.
2. The predicted tension of the sling agrees with the experimental data indicating that the analytical procedure is valid.
3. The analysis shows that the role of the parachute sling is not only to transmit the body force of the payload to the parachute but also to absorb a significant amount of energy during the parachute inflation stage.
4. The sling material must meet both the strength and energy absorption criteria.
5. With current webbing constructions and materials, the energy absorption criteria are more difficult to meet than the strength criteria.
6. The testing procedures developed appear satisfactory in assessing the potential of a yarn for the sling application.
7. Two types of yarns were investigated using our testing procedures. The results show that both Nylon 6 and Nylon 66 have the required properties for a sling material although Nylon 6 exhibits higher damage tolerance than Nylon 66 against various types of loads encountered in the parachute deployment process.

NOMENCLATURE

A_p = Projected area of payload
C_D = Drag coefficient of payload
C_A = Aerodynamic drag coefficient of canopy
D = Diameter of canopy
D_0 = Diameter of fully opened canopy
F_x, F_z = External forces along x, z axes
g, g_c = Local acceleration of gravity, dimensional constant
I_{yy} = Moment of inertia about y axis
K_{ij} = Apparent mass coefficients
M_y = External moment about y axis
M_t = Moments acting on parachute system
m = Mass of parachute system
T = Kinetic energy of parachute system
t = Time
t_0 = Parachute opening time
U, W = Velocity components along x, z axes
V = Volume of parachute canopy
V_t = Translational velocity of parachute

x, y, z = Moving coordinates with parachute
X, Y, Z = Fixed coordinates
Z_s, Z_r = Distances along z axis from origin to mass center of parachute and center of aerodynamic forces
α_{ij} = Components of apparent mass tensor
β = Canopy angle of attack
ε_{ijk} = Permutation symbol
θ = Angle between axis x and axis X
σ_t = Tension in sling

Acknowledgment

The authors want to acknowledge the valuable contributions of the groups who conducted the testings described in this study especially their supervisors Dr. I. Palley at Allied-Signal Inc., Ms. M. Schoppee at Albany International Research Co., in Mansfield, Massachusetts and Mr. F. Savino at U.S. Testing Laboratories in Fairfield, New Jersey.

References

1. C. Tory and R. Ayres, "Computer Model of a Fully Deployed Parachute," *Journal of Aircraft*, **14**(7), 675–679 (July 1977).
2. J. A. Eaton, "Added Mass and the Stability of Parachutes," *Journal of Aircraft*, **19**(5), 414–416 (May 1982).
3. F. M. White and D. F. Wolf, "A Theory of Three-Dimensional Parachute Dynamic Stability," *Journal of Aircraft*, **5**(1), 86–92 (Jan.-Feb. 1968).
4. T. Yavuz and D. J. Cockrell, "Experimental Determination of Parachute Apparent Mass and Its Significance in Predicting Dynamic Stability," AIAA Paper No. 81-1920, 7th Aerodynamic Decelerator and Baloon Technology Conference, 1981.
5. K. F. Doherr and C. Saliaris, "On the Influence of Stochastic and Acceleration Dependent Aerodynamic Forces on the Dynamic Stability of Parachutes," AIAA Paper No. 81-1941, 7th Aerodynamic Decelerator and Balloon Technology Conference, 1981.
6. D. J. Cockrell and K. F. Doherr, "Preliminary Consideration of Parameter Identification Analysis From Parachute Aerodynamic Flight Test Data," AIAA Paper No. 81-1940, 7th Aerodynamic Decelerator and Balloon Technology Conference, 1981.
7. T. Yavuz, "Determining and Accounting for a Parachute Virtual Mass," *Journal of Aircraft*, **26**(5), 432–437 (May 1989).